Development of a Portable Hypoxia Chamber for Ultra-high Dose Rate Laser-Driven Proton Radiobiology Applications

Pankaj Chaudhary (p.chaudhary@qub.ac.uk)
Queen's University Belfast School of Mathematics and Physics https://orcid.org/0000-0002-0381-3635
Deborah Caroline Gwynne
Queen's University Belfast School of Mathematics and Physics Centre for Plasma Physics
Boris Odlozilik
Queen's University Belfast School of Mathematics and Physics Centre for Plasma Physics
Aaron McMurray
Queen's University Belfast School of Mathematics and Physics Centre for Plasma Physics
Giuliana Milluzzo
INFN: Istituto Nazionale di Fisica Nucleare Laboratori Nazionale de Sud Catania, Sicily
Carla Maiorino
Queen's University Belfast
Domenico Doria
ELI-NP: Extreme Light Infrastructure Nuclear Physics
Hamad Ahmed
CLF: Science & Technology Facilities Council Central Laser Facility
Lorenzo Romagnani
LULI: Laboratoire pour l'utilisation des lasers intenses
Aaron Alejo
Queen's University Belfast School of Mathematics and Physics Centre for Plasma Physics
Hersimerjit Padda
University of Strathclyde
James Green
CLF: Science & Technology Facilities Council Central Laser Facility
David Carroll
CLF: Science & Technology Facilities Council Central Laser Facility
Nicola Booth
CLF: Science & Technology Facilities Council Central Laser Facility
Paul McKenna
University of Strathclyde
Satyabrat Karr
Queen's University Belfast School of Mathematics and Physics
Giada Petringa
INFN: Istituto Nazionale di Fisica Nucleare Laboratori Nazionale de Sud Catania Sicily
Roberto Catalano
INFN: Istituto Nazionale di Fisica Nucleare Labaratori nazionale de Sud Catania Sicily
Francesco P Cammaratta
IBFM: Istituto di Bioimmagini e Fisiologia Molecolare Consiglio Nazionale delle Ricerche Catania Sicily
Giuseppe Antonio Pablo Cirrone
INFN: Istituto Nazionale di Fisica Nucleare
Stephen J McMahon
Queen's University Belfast;Patrick G Johnston Centre for Cancer Research
Kevin M. Prise
Queen's University Belfast; Patrick G Johnston Centre for Cancer Research
Marco Borghesi
Queen's University Belfast School of Mathematics and Physics Centre for Plasma Physics

Research

Keywords: Ultra-high dose rate, laser-driven protons, hypoxia, DNA Repair

Posted Date: July 7th, 2021

DOI: https://doi.org/10.21203/rs.3.rs-672312/v1

Abstract

Background

There is currently significant interest in assessing the role of oxygen in the radiobiological effects at ultra-high dose rates. Oxygen modulation is postulated to play a role in the enhanced sparing effect observed in FLASH radiotherapy, where particles are delivered at 40-1000 Gy/s. Furthermore, the development of laser-driven accelerators now enables radiobiology experiments in extreme regimes where dose rates can exceed 10^9 Gy/s, and predicted oxygen depletion effects on cellular response can be tested. Access to appropriate experimental enviroments, allowing measurements under controlled oxygenation conditions, is a key requirement for these studies. We report on the development and application of a bespoke portable hypoxia chamber specifically designed for experiments employing laser-driven sources, but also suitable for comparator studies under FLASH and conventional irradiation conditions.

Materials and Methods

We used oxygen concentration measurements to test the induction of hypoxia and the maintenance capacity of the chambers. Cellular hypoxia induction was verified using hypoxia inducible factor-1α immunostaining. Calibrated radiochromic films and GEANT-4 simulations verified the dosimetry variations inside and outside the chambers. We irradiated hypoxic human skin fibroblasts (AG01522B) and patient-derived glioblastoma (E2) cancer stem cells with laser-driven protons, conventional protons and reference 225 kVp X-rays to quantify DNA DSB damage and repair under hypoxia. We further measured the oxygen enhancement ratio for cell survival exposed to cyclotron-accelerated protons and X-rays in the normal fibroblast and radioresistant GBM stem cells.

Results

Oxygen measurements showed that our chambers maintained a radiobiological hypoxic environment for at least 45 minutes and pathological hypoxia for up to 24 hrs after disconnecting the chambers from the gas supply. We observed a significant reduction in the 53BP1 foci induced by laser-driven protons, conventional protons and X-rays in the hypoxic cells compared to normoxic cells at 30 minutes post-irradiation. Under hypoxic irradiations, the Laser-driven protons induced significant residual DNA DSB damage in hypoxic AG01522 cells compared to the conventional dose rate protons suggesting an important impact of these extreme high dose-rate exposures. We obtained an oxygen enhancement ratio (OER) of 2.1 ± 0.108 and 2.501 ±0.125 respectively for the AG01522 and patient derived GBM stem cells for the X-rays using our hypoxia chambers for irradiation.

Conclusion

We demonstrated the design and application of portable hypoxia chambers for studying cellular radiobiological endpoints after laser-driven protons at ultra-high dose, conventional protons and X-ray exposures. Good levels of reduced oxygen concentration could be maintained in the absence of external gassing to quantify hypoxic effects and the data obtained provided an indication of an enhanced residual DNA DSB damage under hypoxic conditions at ultra-high dose rate compared to the conventional protons or X-rays.

Background

It has been known for many years that oxygen is a key radiation sensitiser and in the absence of oxygen significant radioresistance occurs which limits the effectiveness of radiotherapy(1). Importantly, with increasing linear energy transfer (LET) the radiosensitisation by oxygen reduces even for light ions such as protons(2, 3). Ion beam therapy using high linear energy transfer (LET) particles is recognised as an effective approach for killing radioresistant and hypoxic tumour cells(4–6). Charged particles also provide normal tissue sparing which have enabled dose escalation for better tumour control(7–9). Recent studies, with low LET electrons, have shown that high dose-rate approaches such as FLASH radiotherapy (typically > 100 Gy/s) are promising due to the therapeutic index boost they provide through an enhanced normal tissue sparing (10). While the majority of the FLASH studies have used electrons, protons have also been demonstrated to be effective in sparing the normal tissues at FLASH dose rates (11) and can potentially treat deep seated tumours which is not currently feasible with FLASH electrons. FLASH results have led to a renewed interest in the radiobiological effects at high dose rates, and emerging particle sources provide today opportunities for irradiating samples at dose rate much higher than currently used in FLASH. Ultra-high dose rates (UHDR) in the range of 10^9- 10^{10} Gy/sec have already been achieved by using laser-driven proton accelerators (12–15). While most of the cellular effects at UHDR are still unknown, some effects on the DNA damage and repair have been reported (16) including our own studies (17, 18). A role for Oxygen depletion at high dose rates was first suggested about 50 years ago (19) and recently a number of studies have also suggested that oxygen concentration during irradiation may affect the radiobiological outcome and often result in normal tissue sparing (19–23). A recent modelling study by Petersson *et al* (24) using FLASH electrons suggested that cellular protective effects of FLASH irradiation may not be observed at atmospheric oxygen tension level as doses as high as 10s to 100s Gy will be needed to deplete the significant levels of oxygen.

While studies have been performed with FLASH electrons under various oxygenation conditions(23, 25), information on the radiobiological effects of protons under hypoxia is still limited (26–29) and there are no reports at FLASH and ultra-high dose rates. This could mainly be attributed to the lack of suitable experimental systems, including appropriate hypoxia chambers, enabling such experiments with a variety of radiation sources where constraints related to physical ion beam parameters and cellular physiology make measurements difficult.

Several groups have developed hypoxia chambers for radiobiology studies but most of these chambers can be used successfully only in a horizontal orientation when placed on flat surfaces (27, 30, 31). However, most of the experimental fixed beamlines in the cyclotron research facilities, as well as the laser interaction chambers, have a horizontal orientation that allows cells irradiation only in a vertical position i.e. perpendicular to the beam. In this situation, horizontal chambers may not be suitable as there is a high chance of liquid medium spillage and mixing when multi-well plates or petri-dishes are used. The permanent mounting of hypoxia incubators on a beam line is impractical in many situations due to dosimetry requirements, and a simple lightweight, gas-impermeable, portable chamber capable of maintaining hypoxic environment for long durations would be beneficial. In particular, sample re-oxygenation is an important factor that complicates hypoxic cellular irradiations since, when chambers are disconnected from the gas supply, the samples reoxygenate and the saturation level reaches non-radiobiological hypoxia within minutes. Metsällä *et al* (32) have developed a portable hypoxia chamber equipped with a gas cylinder for controlling multiple samples at a time. While this system has been demonstrated to work for X-ray exposures, due to the materials used in construction of the chamber (aluminium for the 6 well flow divider), it may not be suitable for studying ultra-high dose rate effects, with charged particles and laser-driven protons, under hypoxia due to an impact on dosimetry and the potential for secondary particle generation. Walter *et al* also demonstrated the use of a hypoxia chamber for studies with high LET and high energy carbon, oxygen and nitrogen ions (27, 33). While their hypoxia chamber system was efficient for high energy and high LET particles, the chamber was not tested for the lower energies of relevance to laser-driven protons, where the particle energies used for cellular radiobiology endpoints are often typically ~ 10–20 MeV, with short ranges in air.

The procedures and constraints of laser driven proton irradiation are currently very different than conventional proton beam irradiation using RF accelerator beams. The workflow in a laser-driven proton irradiation procedure is not as fast as in a conventional proton beam experiment. The proton beam is generated inside a high vacuum laser interaction chamber by focussing very high power lasers onto thin targets. Biological samples cannot be irradiated inside the interaction chamber due to the high vacuum (< 1 x 10^{-4} mbar) so the beam needs to be steered out of the interaction chamber using strong magnetic field exiting through a thin Kapton window. This Kapton window acts as a sample irradiation port and is kept isolated from any outside elements by installation of a narrow diameter (20cm) sample re-entry tube perpendicular to the axis of the exit window. This limits the size of cell samples which can be irradiated and only compact hypoxia chambers can be used to control the gassing conditions. The compact hypoxia chambers are introduced on a rail through this narrow tube such that the hypoxia chamber window can align with the Kapton window during the irradiation. Target alignment and radiation safety checks required before each shot significantly increase the set-up time required to prepare for and complete an irradiation compared to conventional proton exposures. The cells, attached as monolayers in the Mylar dishes, cannot be held in upright position for long durations as this may lead to dehydration of the cells. To overcome this problem, we mounted the hypoxia chambers on remotely controlled motorized flippers. Immediately before irradiation, the hypoxia chambers are slowly flipped vertically and after irradiation they are returned to the horizontal position, removed and taken for post irradiation processing. We addressed all these issues during the design and development of a portable hypoxia chamber and successfully used it to measure ultra-high dose-rate laser-driven proton DNA damage and repair under oxic and hypoxic conditions alongside comparator studies with conventional dose rate protons and X-rays. Further, we also measured the oxygen enhancement ratio (OER) for survival of cells irradiated with reference X-rays in the hypoxic chambers. Overall, our results clearly indicate the effectiveness of these hypoxia chambers in the maintenance of hypoxic environment during irradiation with various radiation qualities without adversely affecting the physical and radiobiological readouts.

Materials And Methods

Cell Culture: AG01522B cells were obtained from the Coriell Institute for Medical Research (Camden, New Jersey, USA) and maintained in α-modified Minimum Essential Medium (MEM) (Sigma Aldrich) supplemented with 20% Fetal Bovine Serum (FBS) and 1% penicillin-streptomycin (Thermo Fischer Scientific, Loughborough, UK). These cells were routinely tested for Mycoplasma contamination and have a finite life span. For all our experiments, early passage cells within passage 2–4 after procuring from the Coriell Repository. Glioblastoma stem like cells (E2 cells) were kindly provided by Prof. Anthony Chalmers (University of Glasgow, UK) and have been previously characterized for the expression of stem cell biomarkers such as NG2, Olig2 and Sox-2. These cells are cultured in Advanced Dulbecco's Modified Eagle's Medium/F-12 serum free medium, supplemented with B27, N2, L-Glutamine, heparin, epidermal growth factor and basal fibroblast growth factor (Thermo Fischer Scientific, Loughborough, UK) and were also routinely tested for mycoplasma contamination. Cell culture flasks and cell dishes used for E2 cells were coated with a thin layer of growth factor reduced basement membrane Matrigel (Corning, NY, USA) dissolved in DMEM/F-12 medium at a dilution of 1:40 giving a final concentration of matrigel proteins of 0.225 mg/ml of medium. All the cells were maintained in 5% CO_2 with 95% humidity at 37°C.

Hypoxia chamber design, hypoxia induction and Oxygen measurement

The design and assembly of the hypoxia chamber is shown in Fig. 1(a-e). The main body of the hypoxia chamber is a hollow box made of polyetheretherketone (PEEK) (Direct Plastics, Sheffield, England, UK) sheet of 5 mm with dimensions of 12.0 cm (length) 9.6 cm (width) and 3.8 cm (height). The front and rear faces of the chamber have 4.7 cm diameter circular openings. These openings are sealed with a 12.5 µm oxygen impermeable polyvinylidene chloride (PVDC) or Saran membrane (Goodfellow Cambridge Ltd, Huntingdon, England), attached with 0.4 cm and 0.2 cm thick PEEK rings screwed with silicone 'O' rings underneath for sealing on both the front and rear, creating two transparent windows. Two stainless steel gas ports, one inlet and one outlet, were attached to the right side of the box. These ports were connected to two-way valves with flexible polyurethane tubing. The inlet port extends inside the chamber to the left-hand side of the box to ensure uniform thorough saturation of the chamber with a hypoxia gas mixture.

Oxygen concentration measurements were taken for six independent chambers using an oxygen gas analyser (Rapidox 1100Z, Cambridge Sensotec, Cambridge UK) connected to the chambers in the arrangement shown in Fig. 1(e). Briefly, the chambers were flushed with the hypoxic gas (95 % N_2, 5 % CO_2, BOC Gases, Belfast, UK), for 15 minutes through the inlet port. The outlet from the hypoxia chamber was fed into the inlet port of the oxygen analyser and the outlet of the analyser was connected to a small water-filled flask for visual monitoring of the gas flow rate. The chambers were gassed at a flow rate of 0.5-1 litre per minute until the oxygen saturation dropped down to 0.005–0.01% between 0–3 mm Hg oxygen tension. At this stage, the inlet and outlet valves of the chambers were closed, the oxygen analyser outlet tube was immediately removed from the water-filled flask and attached to the inlet port of the chamber. In this way a closed loop was formed between the hypoxia chamber and the oxygen gas analyser that allowed continuous monitoring of the oxygen concentration inside the chamber for the next 24 hours.

For hypoxia induction the cells were grown inside customized stainless steel dishes with a 3 µm Mylar membrane base for cell attachment(Fig. 1c) which was mounted inside the chamber (Fig. 1d). The whole assembly was then incubated in a cell culture incubator at 37^{o}C where the chambers were continuously gassed for 4 hrs with the hypoxia gas mixture.

Irradiations

Laser-driven protons

Laser-driven protons were generated at the Petawatt arm of the VULCAN laser at the Central Laser Facility of the Rutherford Appleton Laboratory, Didcot, Oxford, UK. Protons were accelerated by focussing the Vulcan Laser at an intensity of order 5-10^{20} W/cm^2 onto a 25 µm-thick aluminium foil. The protons were accelerated through the Target Normal Sheath Acceleration mechanism (34, 35)from the hydrogen contained in a contaminant layer on the rear surface of the target. As typical for this mechanism, the energy spectrum of the accelerated protons was broadband, approximately decreasing exponential, up to a cut-off energy of ~ 30 MeV. The proton irradiation setup was designed to minimize the distance between the target and the cells, compatibility with energy selection and shielding requirements, in order to achieve a suitable dose on the cells on a single-shot basis, as well as to minimize the temporal duration of the ion irradiation. A 1.0 T magnet was used in conjunction with a collimator and pinhole to disperse and spatially select the proton energy and irradiate the cells with the selected 15 ± 1.2 MeV protons. The protons exited the interaction chamber through a flange-mounted 50 µm Kapton window before reaching the cells, located approximately 30 cm away from the laser interaction point at the transversal position corresponding to the 15 MeV proton spatial dispersion. Dose rates of 2 x 10^9 Gy/sec were achieved in single ion pulses of ~ 400 ps duration. Hypoxia chambers with motorised mounts were inserted on a slide rail through a re-entrant tube in a horizontal position to keep the cells submerged in liquid medium. Just prior to firing the laser, the hypoxia chambers were raised slowly from the horizontal to vertical position, so that the cells were precisely in the beam path, through a remotely controlled motorized mount as shown in the Fig. 2 (a-c).

Conventional Dose Rate Protons

Cells were irradiated at conventional dose rate of 4 Gy per minute with the proton beams accelerated by the superconducting cyclotron (CS) along the CATANA proton therapy beam line of Laboratory Nazionale de Sud (LNS), Istituto Nazionale Fisica Nucleare (INFN) Catania, Italy. The 30 MeV proton beam extracted from the CS, was then degraded using a 4 mm-thick PMMA range shifter placed in-air along the beam line, in order to obtain 15 MeV protons at the cell position. Portable hypoxia chambers were mounted inside the Perspex sample holder and aligned on a motorized X-Y translator stage as shown in supplementary figure-1, and movement across X and Y axis was controlled remotely. A 2 cm x 2 cm collimated proton beam irradiated the cells inside the hypoxia chambers and nine collimated fields were used to fully irradiate the cell dish.

X-rays

Cellular irradiations with 225 kVp X-rays were performed in house in our institution using a X-Rad 225 (Precision X-ray, Connecticut, USA), X-ray generator at a dose rate of 0.59 Gy/min. Both hypoxic and normoxic cells were irradiated inside the shielded cabinet for the time duration required to deliver each dose.

Dosimetry and simulations for Hypoxia Chambers

Due to the limited energy of the laser-driven protons used in the irradiation, it is crucial to understand how the different materials in the beam path affect the dosimetry and other beam parameters such as the proton energy spectrum and generation of secondary particles. For dosimetry, a fully assembled Mylar dish, containing an EBT3 film placed under the Mylar adjacent to the cell plane, was placed inside the hypoxia chamber and irradiated with protons as shown in Fig. 2d. The horizontal dose profiles measured with the EBT3 film placed at the cell position inside the chamber (red data points) and outside the chamber (blue data points) are shown in Fig. 2e for comparison. A Monte Carlo GEANT4 simulation was also performed to estimate the proton energy loss through all the traversed materials of the hypoxia chamber, considering as input a narrow band 15 MeV proton beam impinging into the 12.5 um PVDC Saran window. The energy loss is not significant as shown in Fig. 2f. We also confirmed the dosimetry for X-rays as indicated in the supplementary Fig. 1.

Biological Validation of Hypoxia

The hypoxia inducible factor – 1α (HIF-1α) is a well-known biomarker of hypoxia which is expressed upon hypoxia induction in human cells. Using immunofluorescent staining we detected HIF-1α in human skin fibroblasts after hypoxia induction using our chambers. Briefly, the cells were incubated

under the hypoxic gas mixture flow for 4 hours and immediately fixed in 4% paraformaldehyde. Cells were then permeabilized, blocked in 10% goat serum and probed with a mouse primary anti-HIF-1 α antibody (Abcam, Cambridge, UK) and then washed and probed with goat-anti-mouse Alexa flour 594 secondary antibody (ThermoFischer Scientific, UK). Finally, the cells were mounted with antifade reagent containing nuclear stain DAPI.

DNA DSB damage and repair under Hypoxia

We detected DNA DSB damage and repair using the 53BP1 foci formation assay in hypoxic and oxic AG01522 cells irradiated with laser-driven protons, conventional protons and X-rays. Cells were gassed for four hours and then irradiated with either 1 Gy of 15 MeV laser-driven protons, conventional dose rate protons or X-rays. The cells were then fixed in 4 % paraformaldehyde (PFA) for 20 minutes (room temperature) at 0.5- and 24-hours post-irradiation. For co-staining with HIF-1α and 53BP1, after fixation the samples were rinsed with PBS (Phosphate Buffered Saline) and later permeabilized in 0.5 % Triton X-100 (Sigma Aldrich) in PBS for 10 minutes at room temperature and subsequently blocked in 2 ml of blocking buffer (10 % goat serum and 0.25 % Triton X-100 in PBS) at 37°C for 2 hours. After blocking, 1 ml of the primary antibodies mixture, 1:1000 53BP1 (Novus Biologicals, Littleton, CO, USA) and 1:500 HIF-1α (Abcam, Cambridge, UK) diluted in the blocking medium was added to the dishes and incubated at 37°C for 1 hour and then washed three times in PBS containing 0.1 % Triton X-100. The cells were then probed with a mixture of secondary antibodies (goat anti-rabbit-Alexa Fluor 488 and goat anti-mouse-Alexa Fluor 594), at a dilution of 1:1000 respectively in blocking buffer and incubated for 1 hour at 37°C. The samples were then washed and mounted on coverslips using an anti-fade reagent containing DAPI. Cells were then scored for 53BP1 foci in both oxic and hypoxic samples and plotted as mean number of foci per cell for 0.5 and 24 hrs time points.

Oxygen Enhancement Ratio

We used the clonogenic cell survival assay to calculate the oxygen enhancement ratio for normal human skin fibroblasts (AG01522B) and patient derived radioresistant glioblastoma stem like cells (E2 Cells) irradiated with X-rays. Due to the technical difficulties involved in generating radiation doses in the range relevant for cell survival assay as well as large dose spread within beam spots, it was not feasible to conduct cell survival assay with laser-accelerated protons during these studies and for this objective, we limited our experiments to X-rays only. Both the normal and radioresistant cells were plated at a density of 2×10^5 cells per dish on Mylar and incubated for 24 hours. After 24 hours, the cell culture medium was replaced with fresh medium and the dishes mounted inside hypoxia chambers connected to hypoxia gas supply as described previously. After 4 hours of gassing, the valves were closed, the chambers disconnected, and exposed hypoxic cells to various doses of X-rays. Immediately after irradiation, each chamber was opened, and the cells were dissociated and plated following the clonogenic assay protocol (36). After twelve days we quantified the colonies in each well of the six-well plates, plotted dose response curves and calculated oxygen enhancement ratio at doses resulting in 10% (D_{10}),50% (D_{50}) and 90% (D_{90}) surviving fraction for both cell lines to determine the impact of both low and high doses of X-rays.

$OER = D_{10, 50 \text{ or } 90}$ (Hypoxic) / $D_{10, 50 \text{ or } 90\ \%}$ (Oxic)

Where $D_{10, 50 \text{ or } 90\ \% =}$ dose resulting in 10, 50 or 90 % surviving fraction

Data Analysis and Statistics

Oxygen measurements were carried out in five independent replicates and data is shown for individual chambers and as the mean for three chambers for comparison. 53BP1 foci were analysed in at least 100 cells in three replicates and reported as mean values ± standard error of the mean (SEM). Statistical significance analysis comparing the foci induction and cell survival values under oxic and hypoxic conditions was performed using an unpaired T test available in GraphPad Prism software, version 9.1.2 (LaJolla, CA,USA), with a threshold for significance at $P < 0.05$ and $P < 0.01$. For OER calculations, cell survival data from atleast two independent X-rays dose response replicates in AG01522 and E2 cells were obtained and fitted in modified Linear Quadratic fitting of Graphpad Prism software. Various transformants reporting dose resulting in 10 % cell survival (D_{10}), 50% cell survival (D_{50}) and 90% cell survival (D_{90}) were obtained from the fits with 95% confidential intervals(CI). The obtained values for D_{10}, D_{50} and D_{90} under hypoxia were divided with the D_{10}, D_{50} and D_{90} values obtained under normoxic conditions to obtain OER and shown as OER with 5% Error.

Results

Oxygen concentration measurement

We measured oxygen concentrations in six individual hypoxia chambers as shown in Fig. 3. All six chambers maintained a physiological hypoxic environment (2 % O_2(37)) for up to 4 hours after disconnection from the gas supply. These chambers maintained radiobiological hypoxia (≤ 0.4% Oxygen(37)) for at least 45 minutes after disconnection from the gas supply, which provided sufficient time to irradiate and process the samples under radiobiological hypoxia conditions without the risk of re-oxygenation during our experiments.

Biological verification of hypoxia using HIF-1α

We used an immunofluorescent assay to detect HIF-1α in the AG01522 cells after 4 hours hypoxia induction. As shown in Fig. 4, HIF-1α is mainly localized in the nucleus of hypoxic cells while in the oxic samples only faint cytoplasmic staining is seen. We observed clear differences in the intensity of HIF-1α staining under both hypoxic and oxic conditions after 4 hrs of gassing for hypoxia induction and similar changes were also noticed in the cells co-stained with DNA DSB marker 53BP1 and HIF-1α.

DNA DSB damage induction and Repair in hypoxic cells

53BP1 foci formation is regarded as one of the hallmarks of DNA DSB damage along with γ-H2AX(38–41). We detected 53BP1 foci formation in AG01522 cells irradiated with 15 MeV laser-driven protons, conventional protons and X-rays with simultaneous staining of HIF-1α as shown in Fig. 5(a) where the 53BP1 foci are shown in green, HIF-1α in red and nucleus in blue. Quantitative analysis, as shown in Fig. 5(b) clearly indicates the effect of hypoxia on the DSB damage induction. Under oxic conditions, the levels of initial damage at 0.5 hour induced by laser-driven protons, conventional protons and X-rays were similar, with mean 53BP1 foci per cell values of 24.21 ± 3.38, 25.58 ± 2.99 and 24.87 ± 0.76 respectively. Similarly, under hypoxia, the levels of initial DNA DSB damage were similar for laser-driven protons, conventional dose rate protons and X-rays with mean 53BP1 foci levels of 14.16 ± 2.51, 11.86 ± 1.49 and 9.67 ± 1.19. Overall, a decrease in the mean 53BP1 foci per cell clearly show the impact of cellular hypoxia on the DNA DSB damage yields.

At 24 hrs post-irradiation, we detected significant changes ($P < 0.05$) in the mean number of residual 53BP1 foci induced by laser-driven protons under hypoxia with mean foci values of 4.49 ± 0.75 compared to mean values of 1.92 ± 0.51 and 1.77 ± 0.19 for conventional protons and X-rays respectively. The residual foci measured for both conventional protons and X-rays were not significantly different from each other. We further compared the DSB foci induced by laser-driven protons and conventional protons by normalizing 53BP1 foci induction value at 0.5 and 24 hrs to those induced by X-rays defined as relative foci induction (RFI) as the ratio of foci induction by laser-driven or conventional proton to X-rays induced foci at same time point(42) as shown in supplementary figure-2. Laser-driven protons showed a statistically significant ($P < 0.05$) RFI value of 2.42 ± 0.24 compared to the conventional proton RFI value of 1.08 ± 0.14 for the residual (24 hours) 53BP1 foci under hypoxia.

Oxygen Enhancement Ratio in AG01522 and patient-derived GBM stem cells:

We calculated the oxygen enhancement ratio for cell survival of X-rays in both the normal AG01522B cells and E2 cells. Figure 6a shows the AG01522 cell survival curve for oxic and hypoxic conditions and Fig. 6b shows the cell survival curves for E2 cells under oxic and hypoxic conditions. Dose resulting in cell survival at various levels such as D_{10}, D_{50} and D_{90} were obtained for each cell line from the X-rays dose response curve under oxic and hypoxic conditions. The OER varied for each cell line and a dose dependent variation in OER was observed as shown in additional information table-1. For normal human fibroblast cell line AG01522 cells we observed an OER value of 1.799 ± 0.090, 2.037 ± 0.102 and 2.160 ± 0.108 respectively for D_{10}, D_{50} and D_{90}. For radioresistant E2 cells the OER values were 1.84 ± 0.092, 2.245 ± 0.112 and 2.502 ± 0.125. The OER values varied both with the change in dose and the nature of cell lines. Variation in OER as a function of dose and cellular radiosensitivity were also reported by(43, 44).

Discussion

Overcoming hypoxic radioresistance still remains one of the most important unmet challenges even with the most advanced radiotherapy modalities(45). Despite the tremendous progress made in imaging hypoxia (46) and radiotherapy modelling based concepts such as dose and LET painting with charged particles (5, 47, 48) the treatment of hypoxic tumours is still challenging. Radiobiological data on the effectiveness of charged particles under hypoxia is also still very limited. At UHDR above 10^7 Gy/sec, only a few papers are available that show the role of oxygen depletion with electron beams (23) while there is no radiobiological data reported with UHDR protons. In this study, we successfully designed and developed compact portable hypoxia chambers and tested them for maintaining radiobiological hypoxia for extended periods after gassing and being disconnected from the gas supply. As laser-driven proton beam acceleration techniques are still evolving, cellular irradiation with laser -driven beams is not yet optimal in terms of achieving good dose uniformity and the ability to raster scan at speed across a sample in contrast to cyclotron accelerated proton beams. On the other hand, the achievement of UHDR exceeding 10^8 Gy/sec in single pulses of ~ ns duration makes them an ideal approach to access and study novel radiobiological regimes.

Due to accessibility constraints at high-power laser facilities, the time between irradiation of individual samples can vary from several minutes to an hour. Our hypoxia chambers facilitate the maintenance of hypoxia for the entire duration of transportation, alignment, irradiation and transport back to laboratory for post-irradiation processing. Oxygen concentration values relevant to radiobiological, pathological and physiological levels of hypoxia and the hypoxia retention efficiency at all levels of the chambers are shown in Fig. 3. All six hypoxia chambers were able to maintain a physiological hypoxia environment (2 % O_2) for the full 24 hours' test period and radiobiological hypoxia for about 45 minutes after disconnecting from the gas supply.

For reproducible dosimetry, a thin window membrane was used to minimise any impact of charged particle interactions within the chambers which was confirmed with both proton and X-ray exposures. As energy selection is more robust in laser-accelerated protons compared to the dose selection, we used GEANT4 simulation to verify the energy changes inside and outside the hypoxia chamber and found no changes in energy spectrum of the protons as shown in Fig. 2f. Such dosimetry verifications are very important as the aluminium or other components used in chambers upon interaction with protons may produce secondary particles which may either attenuate beam energy or may cause changes in delivered dose and were not reported by previous investigators (27, 33) (32).

Using the chambers, we tested the effects of hypoxia on key radiobiological endpoints such as DNA DSB damage and cell survival for two cell lines. We used AG01522 primary human fibroblasts as they have been extensively used as radiobiological models to represent normal cells (17, 36, 49–53) and patient-derived glioblastoma E2 stem like cells, as a model system for radioresistant cells and have previously been used to evaluate the role of DNA

damage signalling and DNA repair inhibitors in radiation-resistant brain tumours (54–57). In this paper due to the unavailability of the E2 cells at the time of the laser-driven experiments, we limited the DNA DSB damage assay to AG01522 cells, while for cell survival studies with X-rays we used both cell lines.

The main aim of this paper is to show the potential of the designed chamber to maintain radiobiological hypoxic environment during irradiations. Under normoxic conditions, only background cytoplasmic staining of HIF-1α was observed while upon hypoxia induction for 4 hrs, an intense nuclear staining of HIF-1α was clearly detected.

53BP1 foci formation is regarded as one of the hallmarks of DNA DSB damage(39, 40, 53). We detected 53BP1 foci formation in AG01522 cells irradiated with 15 MeV protons, with simultaneous staining of HIF-1α, a hypoxia biomarker, by immunofluorescent microscopy as shown in Fig. 5a. The images show the nuclear localisation of the 53BP1 foci in both the hypoxic and oxic samples. The initial DNA DSB damage yield as confirmed through 53BP1 foci at 0.5 hour did not vary significantly among the cells irradiated with laser-driven protons, conventional dose rate protons or X-rays under normoxic conditions. This confirms other published data using γ-H2AX foci (15) and both γ-H2AX and 53BP1 (55) for 4.5 MeV (15) or 2.1 MeV (55) laser-driven protons, X-rays or cyclotron-accelerated protons(15, 58) under normoxia. In our study, for the first time we also compare laser-driven proton effects under oxic and hypoxic conditions and show residual DNA DSB damage at 24 hrs post-irradiation was significantly higher ($P < 0.05$) in hypoxic cells compared to the oxic AG01522 cells. In contrast, the residual DNA DSB damage levels induced by X-rays and conventional dose rate protons, both under the normoxic and hypoxic conditions were similar.

FLASH studies with electrons under normoxic conditions have always demonstrated no impact on cell killing relative to conventional dose rate exposures *in vitro*, and it is predicted that the observed sparing effects(9, 59) under *in-vivo* conditions are due to differences between normal and tumour tissue as well as oxygenation levels.. In contrast, the higher residual DNA DSB damage under hypoxia observed here with laser-driven protons clearly suggests a dose rate effect, which has not so far been reported. As residual DNA DSB damage observed through persistent γ-H2AX foci has been associated with late normal tissue toxicity(60), it is reasonable to infer that the higher residual 53BP1 foci levels measured under hypoxia may result in enhanced cell killing. Enhanced cell killing under hypoxia would clearly lead to improved tumour control as hypoxia is a prominent feature of solid tumours(61) in contrast to normal tissues which may become transiently hypoxic during the irradiation (due to local oxygen depletion if the dose/dose-rate is high enough). This warrants further investigation and confirmation of the yields of DNA DSB damage induced by laser-driven proton under hypoxia, and, for a more comprehensive assessment of the effect, future studies should include comparisons in a wider range of models.

As DNA DSB damage is a key mediator of cell-death, we also tested whether the hypoxic environment inside the chambers has any impact on cell survival. OER is a widely used parameter(28, 62) under both clinical and pre-clinical settings to quantify oxygen sensitisation(36, 63–65). We quantified the OER for cell survival of the AG01522 and patient derived E2 GBM stem cells following X-rays irradiation. As shown in Fig. 6a and 6b the dose response curve of the two cell lines differs due to their intrinsic radiosensitivity. The OER value for the AG01522B cells was 2.16 ± 0.108 lower than that measured for the radioresistant E2 cells 2.501 ± 0.125 at D_{90}. These results clearly showed that our compact portable hypoxia chambers efficiently maintained the hypoxic environments for the duration of irradiation and sample transport for further processing. Our hypoxia chambers, once gassed, can be used as a standalone unit unlike the previously developed systems, which rely on continuous gassing (32), and can result in a bulky system. Thanks to its portability and bespoke design, our hypoxia chambers enabled the first radiobiology measurements under controlled oxygen conditions employing laser driven protons, as well as allowing comparator measurements employing conventional dose rate protons and X-rays.

Conclusions

In this manuscript, we have described the development of a portable hypoxia chamber specifically designed for use in radiobiology experiments in ultra-high dose rates regimes employing beams of laser-driven protons. We have also presented the chamber's successful application to the study of radiobiological endpoints such as DNA DSB damage and cell survival employing not only laser-driven protons, but also conventional proton and X-ray sources for reference studies. Our results indicate similarities with previously published data but also provide a novel benchmark indicating higher residual DNA DSB damage inflicted by laser-driven UHDR protons under hypoxia compared to cyclotron-accelerated protons.

Declarations

Ethics approval and consent to participate

Not Applicable

Consent for publication

Not applicable

Availability of data and materials

Raw data can be available upon request from the Corresponding authors.

Competing interests

Authors declare no financial or economic competing interests.

Funding:

Authors acknowledge the funding received from the Engineering and Physical Sciences Research Council (EPSRC), through Grants EP/K022415/1, EPJ500094/1 and

EP/P010059/1. This work has also been partly supported by project 18HLT04 UHD pulse, which has received funding from the EMPIR programme co-financed by the Participating States and from the European Union's Horizon 2020 Research and Innovation Programme. Additionally, Boris Odlozilik acknowledges funding from the European Union's Horizon 2020 research and innovation program under the Marie Sklowdowska-Curie grant agreement no 754507. KMP acknowledges support from Brainwaves NI. Aaron McMurray acknowledges the funding support provided by Department for the Economy, Northern Ireland.

Authors' contributions: PC, MB, KMP conceptualized the study. MB, KMP and PMcK wrote the project. PC, DG and DD designed the hypoxia chambers. PC, DG, BO, AM and CM performed physical and biological measurements, analysed the data. PC, DG, MB and KMP wrote the manuscript. DD, HA, LR, AA, HP, GM and SK set-up the experiment, and generated and characterized the laser-driven protons.GM carried out Monte Carlo simulations and obtained various parameters. SJM helped with OER calculation fittings in Prizm software. JG, NB and DC facilitated and supported the experiments in Rutherford Appleton Laboratory and GAP provided the facility and supported experiments with cyclotron-accelerated protons.

Acknowledgements The authors are thankful to Stephen Barnard (Public Health England, Chilton, UK), Stan Botchway (Research Complex at Harwell), Chantal Fowler (Central Laser Facility), Sarah Grattan (Research Complex at Harwell) and Graham Holliman (Public Health England), as well as the workshop staff of Queen's University Belfast and the Central Laser Facility. We sincerely thank Prof Anthony Chalmers and Prof. Colin Watts for providing patient-derived GBM stem cells.

Competing Interests

The authors declare no competing financial and non-financial interests.

References

1. Gray LH, Conger AD, Ebert M, Hornsey S, Scott OC. The concentration of oxygen dissolved in tissues at the time of irradiation as a factor in radiotherapy. Br J Radiol. 1953 Dec;26(312):638–48. Available from: https://www.birpublications.org/doi/epdf/10.1259/0007-1285-26-312-638

2. Barendsen GW. Responses of cultured cells, tumours and normal tissues to radiations of different linear energy transfer. pp 293-356 Curr Top Radiat Res Vol IV Ebert, Michael Howard, Alma (eds) New York, John Wiley Sons, Inc, 1968 [Internet]. Available from: https://www.osti.gov/biblio/4500126

3. Prise KM, Folkard M, Davies S, Michael BD. The Irradiation of V79 Mammalian Cells by Protons with Energies below 2 MeV. Part II. Measurement of Oxygen Enhancement Ratios and DNA Damage. Int J Radiat Biol [Internet]. 1990 Jan 1;58(2):261–77. Available from: https://doi.org/10.1080/09553009014551611

4. Nakano T, Suzuki Y, Ohno T, Kato S, Suzuki M, Morita S, et al. Carbon beam therapy overcomes the radiation resistance of uterine cervical cancer originating from hypoxia. Clin Cancer Res. 2006;12:2185–90.Available from: https://clincancerres.aacrjournals.org/content/clincanres/12/7/2185.full.pdf

5. Bassler N, Jäkel O, Søndergaard CS, Petersen JB. Dose- and LET-painting with particle therapy. Acta Oncol. 2010;49(July):1170–6. Available from: https://www.tandfonline.com/doi/pdf/10.3109/0284186X.2010.510640?needAccess=true

6. Hirayama R, Furusawa Y, Fukawa T, Ando K. Repair kinetics of DNA-DSB induced by X-rays or carbon ions under oxic and hypoxic conditions. J Radiat Res. 2005;46(3):325–32. Available rom: https://doi.org/10.1269/jrr.46.325

7. Mohan R, Grosshans D. Proton therapy – Present and future. Adv Drug Deliv Rev [Internet]. 2017;109:26–44. Available from: http://dx.doi.org/10.1016/j.addr.2016.11.006

8. Fowler JF. What can we expect from dose escalation using proton beams? Clin Oncol. 2003;15(1):10–5. Available from: https://reader.elsevier.com/reader/sd/pii/S0936655502901822?token=DEC9BA131603F312B5FF17AEF4B42FF8D66E872C3B08FFD2064192520F887FA48723821AC97D9D5480CA905D911071ED&originRegion=eu-west-1&originCreation=20210629140944

9. Montay-Gruel P, Acharya MM, Petersson K, Alikhani L, Yakkala C, Allen BD, et al. Long-term neurocognitive benefits of FLASH radiotherapy driven by reduced reactive oxygen species. Proc Natl Acad Sci U S A. 2019;166(22):10943–51. Available from: https://doi.org/10.1073/pnas.1901777116

10. Montay-Gruel P, Meziani L, Yakkala C, Vozenin MC. Expanding the therapeutic index of radiation therapy by normal tissue protection. Br J Radiol. 2019;92(1093). Available from: https://doi.org/10.1259/bjr.20180008

11. Diffenderfer ES, Verginadis II, Kim MM, Shoniyozov K, Velalopoulou A, Goia D, et al. Design, Implementation, and in Vivo Validation of a Novel Proton FLASH Radiation Therapy System. Int J Radiat Oncol Biol Phys [Internet]. 2020;106(2):440–8. Available from: https://doi.org/10.1016/j.ijrobp.2019.10.049

12. Doria D, Kakolee KF, Kar S, Litt SK, Fiorini F, Ahmed H, et al. Biological effectiveness on live cells of laser driven protons at dose rates exceeding 109 Gy/s. AIP Adv. 2012;2(1). Available from: https://doi.org/10.1063/1.3699063

13. Yogo A, Maeda T, Hori T, Sakaki H, Ogura K, Nishiuchi M, et al. Measurement of relative biological effectiveness of protons in human cancer cells using a laser-driven quasimonoenergetic proton beamline. Appl Phys Lett [Internet]. 2011 Jan 31;98(5):053701. Available from: http://aip.scitation.org/doi/10.1063/1.3551623

14. Zeil K, Baumann M, Beyreuther E, Burris-Mog T, Cowan TE, Enghardt W, et al. Dose-controlled irradiation of cancer cells with laser-accelerated proton pulses. Appl Phys B Lasers Opt. 2013;110(4):437–44.

15. Bin J, Allinger K, Assmann W, Dollinger G, Drexler GA, Friedl AA, et al. A laser-driven nanosecond proton source for radiobiological studies. Appl Phys Lett. 2012;101(24). Available from: https://doi.org/ 10.1007/s00340-012-5275-3

16. Cygler J, Klassen N, Ross C, Bichay T, Raaphorst G. The survival of aerobic and anoxic human glioma and melanoma cells after irradiation at ultrahigh and clinical dose rates. Radiat Res [Internet]. 1994;140(1):79–84. Available from: http://www.ncbi.nlm.nih.gov/entrez/query.fcgi?cmd=Retrieve&db=PubMed&%2338;dopt=Citation&%2338;list_uids=7938458

17. Hanton F, Chaudhary P, Doria D, Gwynne D, Maiorino C, Scullion C, et al. DNA DSB Repair Dynamics following Irradiation with Laser- Driven Protons at Ultra-High Dose Rates. Sci Rep [Internet]. 2019;(February):1–10. Available from: http://dx.doi.org/10.1038/s41598-019-40339-6

18. Manti L, Perozziello FM, Borghesi M, Candiano G, Chaudhary P, Cirrone GAP, et al. The radiobiology of laser-driven particle beams: focus on sub-lethal responses of normal human cells. J Instrum [Internet]. 2017;12(03):C03084. Available from: http://stacks.iop.org/1748-0221/12/i=03/a=C03084

19. Weiss H, Epp ER, Heslin JM, Ling CC, Santomasso A. Oxygen Depletion in Cells Irradiated at Ultra-high Dose-rates and at Conventional Dose-rates. Int J Radiat Biol Relat Stud Physics, Chem Med [Internet]. 1974 Jan 1;26(1):17–29. Available from: https://doi.org/10.1080/09553007414550901

20. Durante M, Brauer-Krisch E, Hill M. Faster and safer? FLASH ultra-high dose rate in radiotherapy. Br J Radiol [Internet]. 2017;(November 2017):20170628. Available from: http://www.ncbi.nlm.nih.gov/pubmed/29172684%0Ahttp://www.birpublications.org/doi/10.1259/bjr.20170628

21. Favaudon V, Caplier L, Monceau V, Pouzoulet F, Sayarath M, Fouillade C, et al. Ultrahigh dose-rate FLASH irradiation increases the differential response between normal and tumor tissue in mice. Sci Transl Med. 2014;6(245):1–10.Available from:https://doi.org/10.1126/scitranslmed.3008973

22. Montay-Gruel P, Petersson K, Jaccard M, Boivin G, Germond JF, Petit B, et al. Irradiation in a flash: Unique sparing of memory in mice after whole brain irradiation with dose rates above 100Gy/s. Radiother Oncol [Internet]. 2016;124(3):365–9. Available from: http://dx.doi.org/10.1016/j.radonc.2017.05.003

23. Adrian G, Konradsson E, Lempart M, Bäck S, Ceberg C, Petersson K. The FLASH effect depends on oxygen concentration. Br J Radiol. 2020;93(1106). Available from: https://doi.org/10.1259/bjr.20190702

24. Petersson K, Adrian G, Butterworth K, McMahon SJ. A Quantitative Analysis of the Role of Oxygen Tension in FLASH Radiation Therapy. Int J Radiat Oncol Biol Phys [Internet]. 2020;107(3):539–47. Available from: https://doi.org/10.1016/j.ijrobp.2020.02.634

25. Khan S, Bassenne M, Wang J, Manjappa R, Melemenidis S, Breitkreutz DY, et al. Multicellular spheroids as in vitro models of oxygen depletion during FLASH irradiation. Int J Radiat Oncol [Internet]. 2021;1–12. Available from: https://doi.org/10.1016/j.ijrobp.2021.01.050

26. Lee, Kheun Byeol,Kim Kye-Ryung H tae-L and LMY. Proton induces apoptosis of hypoxic tumor cells by the p53-dependent and p38/JNK MAPK signalling pathways. Int J Oncol [Internet]. 2008;33:1247–56. Available from: https://doi.org/10.3892/ijo_00000115

27. Ma NY, Tinganelli W, Maier A, Durante M, Kraft-Weyrather W. Influence of chronic hypoxia and radiation quality on cell survival. J Radiat Res. 2013;54:13–22. Available from: https://doi.org/10.1093/jrr/rrs135

28. Tinganelli W, Durante M, Hirayama R, Krämer M, Maier A, Kraft-Weyrather W, et al. Kill-painting of hypoxic tumours in charged particle therapy. Sci Rep. 2015;5:1–13. Available from: https://doi.org/ 10.1038/srep17016

29. Kanemoto a., Hirayama R, Moritake T, Furusawa Y, Sun L, Sakae T, et al. RBE and OER within the spread-out Bragg peak for proton beam therapy: in vitro study at the Proton Medical Research Center at the University of Tsukuba. J Radiat Res [Internet]. 2014;55(5):1028–32. Available from: http://jrr.oxfordjournals.org/cgi/doi/10.1093/jrr/rru043

30. Kumareswaran R, Ludkovski O, Meng a., Sykes J, Pintilie M, Bristow RG. Chronic hypoxia compromises repair of DNA double-strand breaks to drive genetic instability. J Cell Sci. 2012;125:189–99. Available from: https://doi.org/ 10.1242/jcs.092262

31. Vordermark D, Menke DR, Brown JM, Ma N-YN-Y, Tinganelli W, Maier A, et al. Similar Radiation Sensitivities of Acutely and Chronically Hypoxic Cells in HT 1080 Fibrosarcoma Xenografts. Nat Rev Cancer [Internet]. 2013 Jul 1 [cited 2014 Jul 21];4(1):443–7. Available from: http://dx.doi.org/10.1016/j.jscs.2010.02.005

32. Metsälä O, Kreutzer J, Högel H, Miikkulainen P, Kallio P, Jaakkola PM. Transportable system enabling multiple irradiation studies under simultaneous hypoxia in vitro. Radiat Oncol. 2018;13(1):220. Available from: 3:220 https://doi.org/10.1186/s13014-018-1169-9

33. Tinganelli W, Ma NY, Von Neubeck C, Maier A, Schicker C, Kraft-Weyrather W, et al. Influence of acute hypoxia and radiation quality on cell survival. J Radiat Res. 2013;54(SUPPL.1):23–30. Available from:https://doi.org/ 10.1093/jrr/rrt065

34. Snavely R a, Key MH, Hatchett SP, Cowan TE, Roth M, Phillips TW, et al. Intense high-energy proton beams from Petawatt-laser irradiation of solids. Phys Rev Lett [Internet]. 2000 Oct 2;85(14):2945–8. Available from: http://www.ncbi.nlm.nih.gov/pubmed/11005974

35. Macchi A, Borghesi M, Passoni M. Ion acceleration by superintense laser-plasma interaction. Rev Mod Phys [Internet]. 2013 May [cited 2013 Aug 19];85(2):751–93. Available from: http://link.aps.org/doi/10.1103/RevModPhys.85.751

36. Chaudhary P, Marshall TI, Perozziello FM, Manti L, Currell FJ, Hanton F, et al. Relative biological effectiveness variation along monoenergetic and modulated Bragg peaks of a 62-MeV therapeutic proton beam: A preclinical assessment. Int J Radiat Oncol Biol Phys. 2014;90(1). Available from:https://doi.org/ 10.1016/j.ijrobp.2014.05.010

37. McKeown SR. Defining normoxia, physoxia and hypoxia in tumours-implications for treatment response. Br J Radiol. 2014;87(October 2013):20130676. Available from: https://www.birpublications.org/doi/10.1259/bjr.20130676

38. Neumaier T, Swenson J, Pham C, Polyzos a., Lo a. T, Yang P, et al. From the Cover: Evidence for formation of DNA repair centers and dose-response nonlinearity in human cells. Proc Natl Acad Sci. 2012;109(2):443–8. Available from: https://www.pnas.org/content/109/2/443

39. Asaithamby A, Chen DJ. Cellular responses to DNA double-strand breaks after low-dose gamma-irradiation. Nucleic Acids Res [Internet]. 2009 Jul [cited 2012 Oct 26];37(12):3912–23. Available from: http://www.pubmedcentral.nih.gov/articlerender.fcgi?artid=2709554&tool=pmcentrez&rendertype=abstract

40. Panier S, Boulton SJ. Double-strand break repair: 53BP1 comes into focus. Nat Rev Mol Cell Biol [Internet]. 2014 Jan [cited 2014 Jul 10];15(1):7–18. Available from: http://www.ncbi.nlm.nih.gov/pubmed/24326623

41. Zimmermann M, de Lange T. 53BP1: pro choice in DNA repair. Trends Cell Biol [Internet]. 2014 Feb [cited 2014 Jul 14];24(2):108–17. Available from: http://www.ncbi.nlm.nih.gov/pubmed/24094932

42. Hanton F, Chaudhary P, Doria D, Gwynne D, Maiorino C, Scullion C, et al. DNA DSB Repair Dynamics following Irradiation with Laser-Driven Protons at Ultra-High Dose Rates. Sci Rep. 2019;9(1). Available from: https://www.nature.com/articles/s41598-019-40339-6.pdf

43. Freyer JP, Jarrett K, Carpenter S, Raju MR. Oxygen enhancement ratio as a function of dose and cell cycle phase for radiation-resistant and sensitive CHO cells. Radiat Res. 1991;127(3):297–307. Available from: https://pubmed.ncbi.nlm.nih.gov/1886986/

44. Wenzl T, Wilkens JJ. Theoretical analysis of the dose dependence of the oxygen enhancement ratio and its relevance for clinical applications. Radiat Oncol. 2011;6(1):1–9. Available from: https://ro-journal.biomedcentral.com/track/pdf/10.1186/1748-717X-6-171.pdf

45. Burroughs SK, Kaluz S, Wang D, Wang K, Meir EG Van, Wang B. Hypoxia inducible factor pathway inhibitors as anticancer therapeutics. Future Med Chem 2014;5(5):1–31. Available from: https://doi.org/10.4155/fmc.13.17

46. Busk M, Overgaard J, Horsman MR. Imaging of Tumor Hypoxia for Radiotherapy: Current Status and Future Directions. Semin Nucl Med. 2020;50(6):562–83. availbe from: https;//doi.org/ 10.1053/j.semnuclmed.2020.05.003

47. Malinen E, Søvik Å. Dose or LET painting - What is optimal in particle therapy of hypoxic tumors? Acta Oncol (Madr). 2015;54(9):1614–22. Available from: https://doi.org/10.3109/0284186X.2015.1062540

48. Chang JH, Wada M, Anderson NJ, Lim Joon D, Lee ST, Gong SJ, et al. Hypoxia-targeted radiotherapy dose painting for head and neck cancer using (18)F-FMISO PET: a biological modeling study. Acta Oncol [Internet]. 2013;52(December 2012):1723–9. Available from: http://www.ncbi.nlm.nih.gov/pubmed/23317145

49. Marshall TI, Chaudhary P, Michaelidesová A, Vachelová J, Davídková M, Vondráček V, et al. Investigating the Implications of a Variable RBE on Proton Dose Fractionation Across a Clinical Pencil Beam Scanned Spread-Out Bragg Peak. Int J Radiat Oncol Biol Phys. 2016;95(1):70–7. Available from: https://doi.org/10.1016/j.ijrobp.2016.02.029

50. Yang H, Anzenberg V, Held KD. The time dependence of bystander responses induced by iron-ion radiation in normal human skin fibroblasts. Radiat Res. 2007;168(3):292–8. Available from:https://doi.org/ 10.1667/RR0864.1

51. Shao C, Prise KM, Folkard M. Signaling factors for irradiated glioma cells induced bystander responses in fibroblasts. Mutat Res - Fundam Mol Mech Mutagen. 2008;638(1–2):139–45. Available from: https://doi.org/10.1016/j.mrfmmm.2007.09.007

52. Nieri D, Berardinelli F, Sgura A, Cherubini R, De Nadal V, Gerardi S, et al. Cyogenetics effects in AG01522 human primary fibroblasts exposed to low doses of radiations with different quality. Int J Radiat Biol [Internet]. 2013 Sep [cited 2014 Jul 23];89(9):698–707. Available from: http://www.ncbi.nlm.nih.gov/pubmed/23607438

53. Chaudhary P, Marshall TI, Currell FJ, Kacperek A, Schettino G, Prise KM. Variations in the Processing of DNA Double-Strand Breaks Along 60-MeV Therapeutic Proton Beams. Int J Radiat Oncol Biol Phys. 2016;95(1):86–94. Available from: https://doi.org/10.1016/j.ijrobp.2015.07.2279

54. Ahmed U, Carruthers R, Gilmour L, Yildirim S, Watts C, Chalmers AJ. Selective Inhibition of Parallel DNA Damage Response Pathways Optimizes Radiosensitization of Glioblastoma Stem-like Cells. 2015;75(21). Available from: https://doi.org/10.1158/0008-5472.CAN-14-3790

55. Carruthers R, Ahmed SU, Strathdee K, Gomez-roman N, Amoah-buahin E, Watts C, et al. ScienceDirect Abrogation of radioresistance in glioblastoma stem-like cells by inhibition of ATM kinase. Mol Oncol [Internet]. 2014;9(1):192–203. Available from: http://dx.doi.org/10.1016/j.molonc.2014.08.003

56. Mannino M, Gomez-roman N, Hochegger H, Chalmers AJ. ScienceDirect Differential sensitivity of Glioma stem cells to Aurora kinase A inhibitors : Implications for stem cell mitosis and centrosome dynamics. Stem Cell Res [Internet]. 2014;13(1):135–43. Available from: http://dx.doi.org/10.1016/j.scr.2014.05.001

57. Gomez-Roman N, Stevenson K, Gilmour L, Hamilton G, Chalmers AJ. A novel 3D human glioblastoma cell culture system for modeling drug and radiation responses. Neuro Oncol. 2017;19(2):229–41. Available from: https://doi.org/10.1093/neuonc/now164

58. Raschke S, Spickermann S, Toncian T, Swantusch M, Boeker J, Giesen U, et al. Ultra-short laser-accelerated proton pulses have similar DNA-damaging effectiveness but produce less immediate nitroxidative stress than conventional proton beams. Sci Rep [Internet]. 2016;6(1):32441. Available from: http://www.nature.com/articles/srep32441

59. Montay-Gruel P, Petersson K, Jaccard M, Boivin G, Germond JF, Petit B, et al. Irradiation in a flash: Unique sparing of memory in mice after whole brain irradiation with dose rates above 100 Gy/s. Radiother Oncol [Internet]. 2017;124(3):365–9. Available from: http://dx.doi.org/10.1016/j.radonc.2017.05.003

60. Bourton EC, Plowman PN, Smith D, Arlett CF, Parris CN. Prolonged expression of the γ-H2AX DNA repair biomarker correlates with excess acute and chronic toxicity from radiotherapy treatment. Int J Cancer [Internet]. 2011 Dec 15 [cited 2014 Oct 2];129(12):2928–34. Available from: http://www.pubmedcentral.nih.gov/articlerender.fcgi?artid=3427882&tool=pmcentrez&rendertype=abstract

61. Najafi M, Farhood B, Mortezaee K, Kharazinejad E, Majidpoor J, Ahadi R. Hypoxia in solid tumors: a key promoter of cancer stem cell (CSC) resistance. J Cancer Res Clin Oncol [Internet]. 2020;146(1):19–31. Available from: https://doi.org/10.1007/s00432-019-03080-1

62. Antonovic L, Lindblom E, Dasu A, Bassler N, Furusawa Y, Toma-Dasu I. Clinical oxygen enhancement ratio of tumors in carbon ion radiotherapy: the influence of local oxygenation changes. J Radiat Res [Internet]. 2014;(April):1–10. Available from: http://www.ncbi.nlm.nih.gov/pubmed/24728013

63. Puck TT, Marcus PI. Action of X-rays on mammalian cells. J Exp Med

. 1956 May 1;103(5):653-66.Available from:https://doi.org/10.1084/jem.103.5.653

64. Butterworth KT, McGarry CK, Clasie B, Carabe-Fernandez A, Schuemann J, Depauw N, et al. Relative biological effectiveness (RBE) and out-of-field cell survival responses to passive scattering and pencil beam scanning proton beam deliveries. Phys Med Biol [Internet]. 2012 Oct 21 [cited 2013 Aug 5];57(20):6671–80. Available from: http://www.ncbi.nlm.nih.gov/pubmed/23022765

65. Thompson HF, Butterworth KT, McMahon SJ, Ghita M, Hounsell AR, Prise KM. The Impact of Hypoxia on Out-of-Field Cell Survival after Exposure to Modulated Radiation Fields. Radiat Res. 2017;188(6):716–24. Available from:https://doi.org/ 10.1667/RR14836.1

Figures

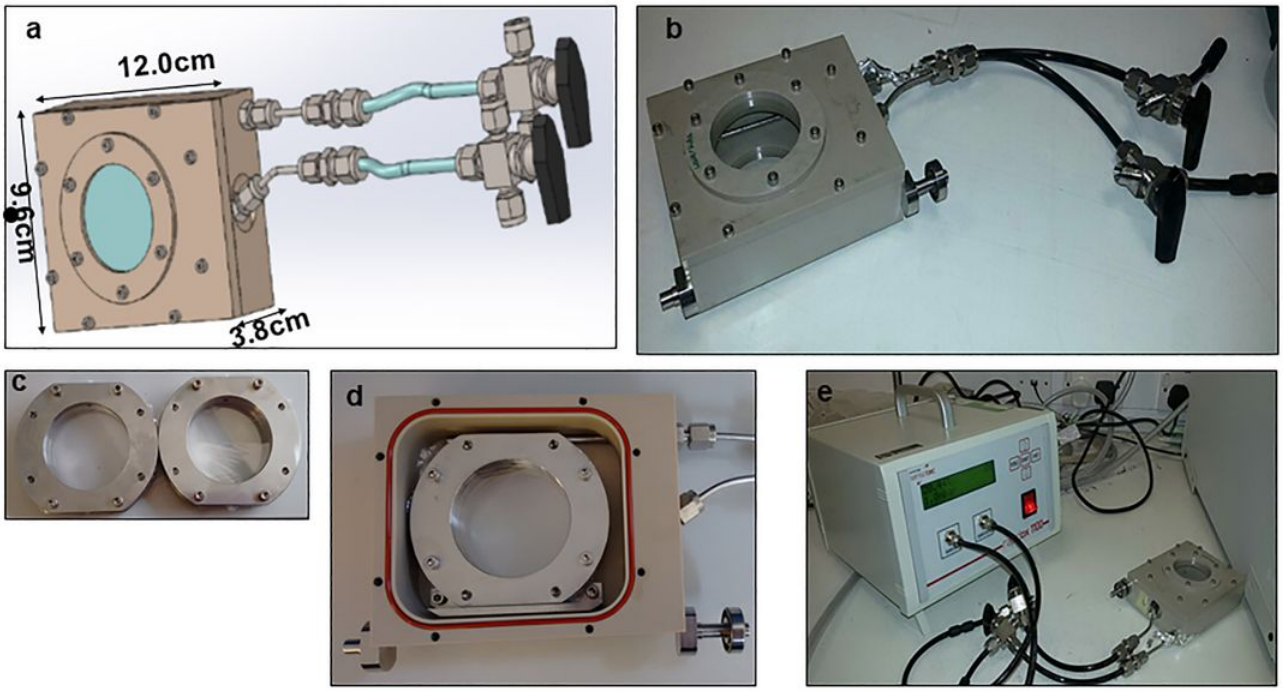

Figure 1

(a) Schematic of the hypoxia chamber. (b) Manufactured hypoxia chamber with the inlet and outlet valves connected to the tubing. Gas impermeable 12μm transparent PVDC window allows visual alignment and irradiation with low energy protons. (c) Stainless-steel dishes mounted with 3μm Mylar for growing cells in monolayers and irradiating with low energy protons. (d) Assembly of the stainless-steel dish inside hypoxia chamber which can be sealed with a lid and mounted on a motorized stage. (e) Arrangement used for measuring the oxygen concentrations over time after gassing the hypoxia chambers using a Rapidox 1100Z detector (Cambridge Sensotec, Cambridge UK).

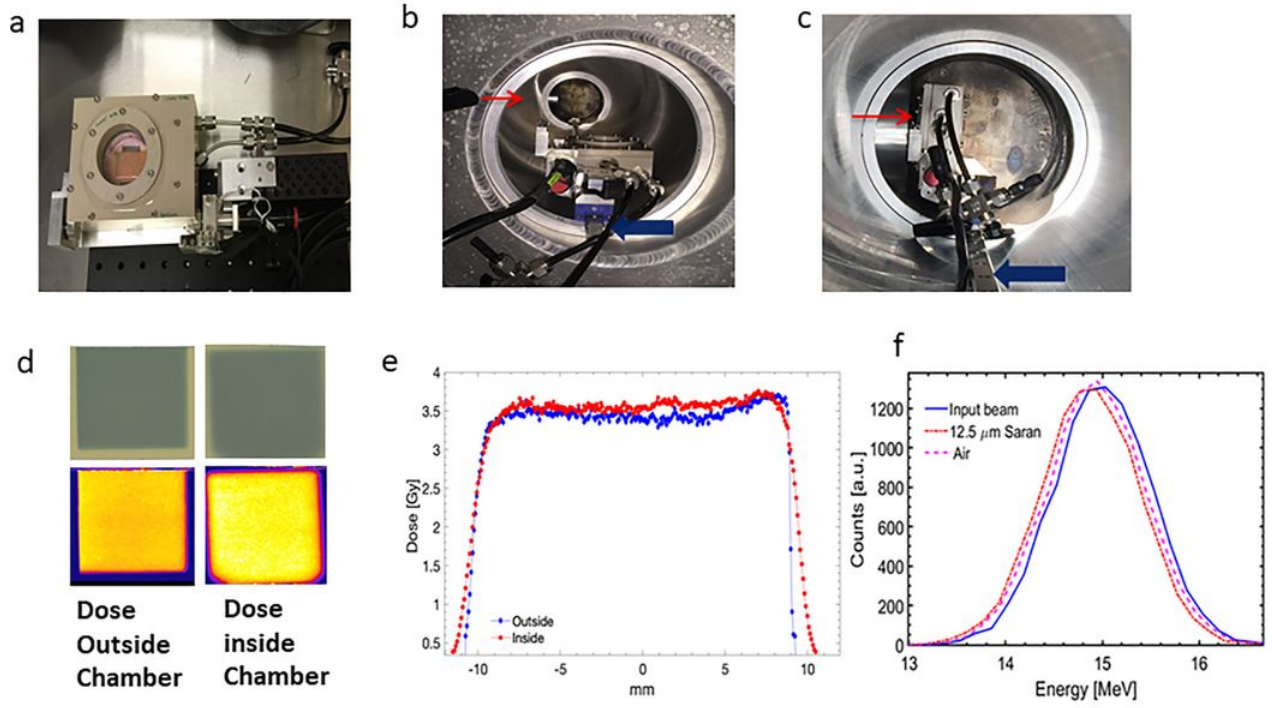

Figure 2

(a) Hypoxia chamber assembled with the cell dish. (b) Irradiation set up of hypoxia chamber inside the re-entry tube. The chamber is slid on the metal rail (blue arrows) towards the end of the tube and just before and during radiation the chamber is tilted vertically as shown in (c) using a motorized mount such that the transparent PVDC window of the hypoxia chamber is facing the Kapton window through which the laser accelerated proton beam emerges and irradiates the cells grown on the Mylar mounted in a stainless steel dish inside the hypoxia chambers.(d) Dose validation inside and outside hypoxia chambers. For each datapoint at least three EBT films were exposed with 15 MeV protons and the data shown represents the mean dose from 3 EBT films. (e) Dose inside the chamber is represented in red and outside the hypoxia chamber is shown in blue. (f) Energy spectra of proton beam in air compared with the proton beam impinging on the 12.5 μm Saran window of the hypoxia chamber obtained using GEANT 4 Monte Carlo Simulation. No significant difference was observed between beam dose and energy inside and outside of hypoxia chamber.

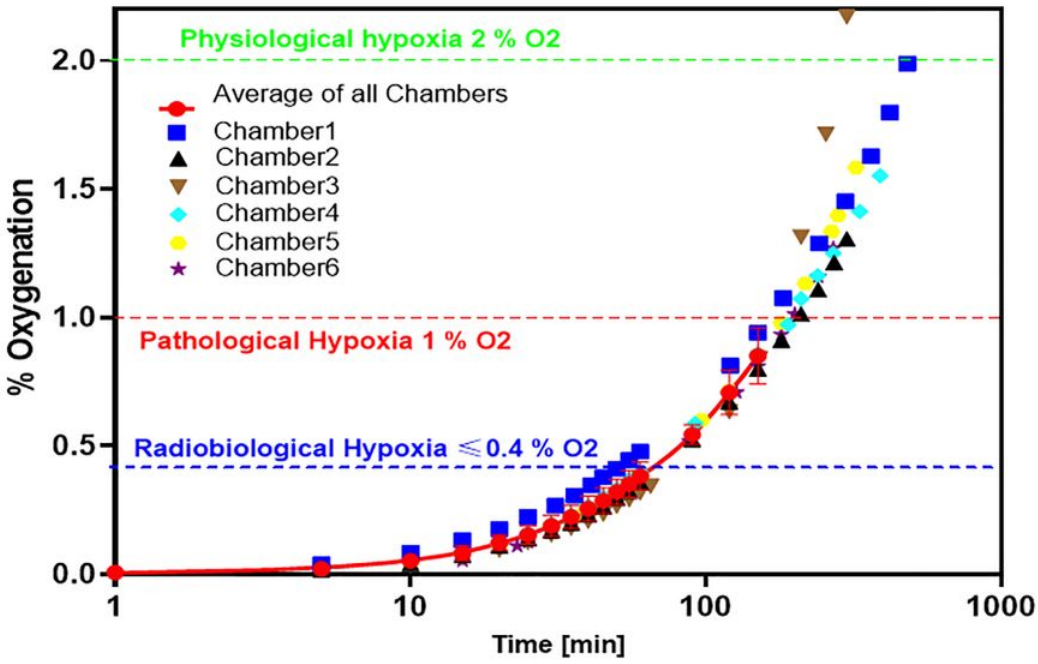

Figure 3

Physical validation of hypoxia as carried out using an Oxygen sensing probe. (a) Oxygen concentration measurement over the period of 24 hrs after gassing the chambers. (b) Detailed view of the oxygen concentration during the first 100 minutes.(c) Average values of the oxygen concentration from all three chambers over 24 hrs. After gassing the chambers were connected to the Rapidox meter and readings were taken every 5 minutes for the first 30 minutes and then every 30 minutes for next 6 hours and then every 2 hours until 24 hrs. Values of various types of hypoxia- physiological, pathological and radiobiological are shown through solid or dashed lines in each figure. For the initial 30 minutes after gassing, all the chambers maintained the oxygen level below 0.4% (radiobiological hypoxia) providing, enough time to allow sample alignment and irradiation with laser-driven protons, conventional protons or X-rays.

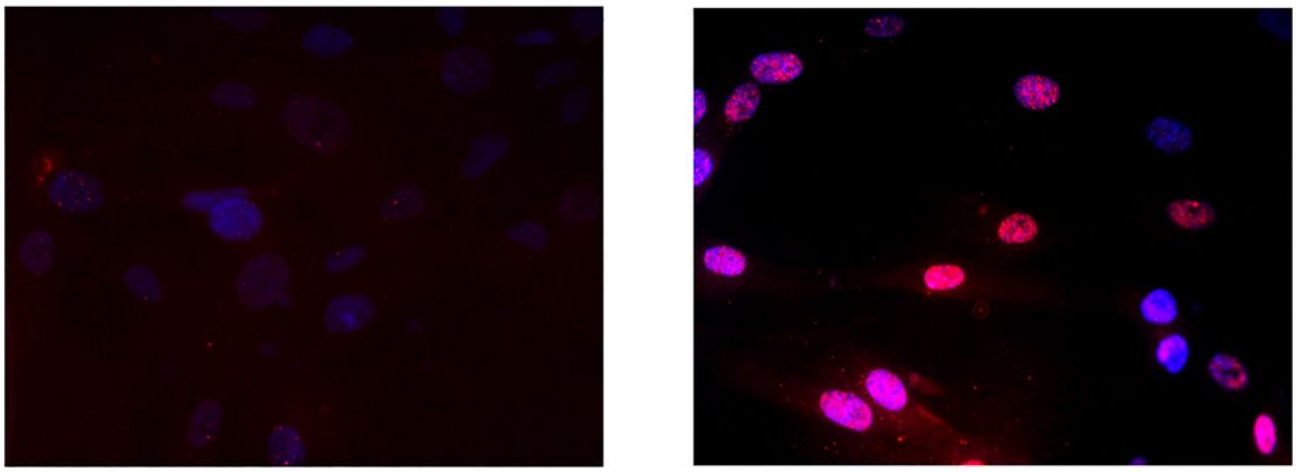

Figure 4

Immunofluorescent detection of hypoxia induction in AG01522B cells after 4 hours of gassing with 95% nitrogen and 5% CO_2 inside hypoxia chambers. HIF-1 α was detected using primary anti-HIF-1α antibody later probed with secondary Alexa fluor 594 antibody.

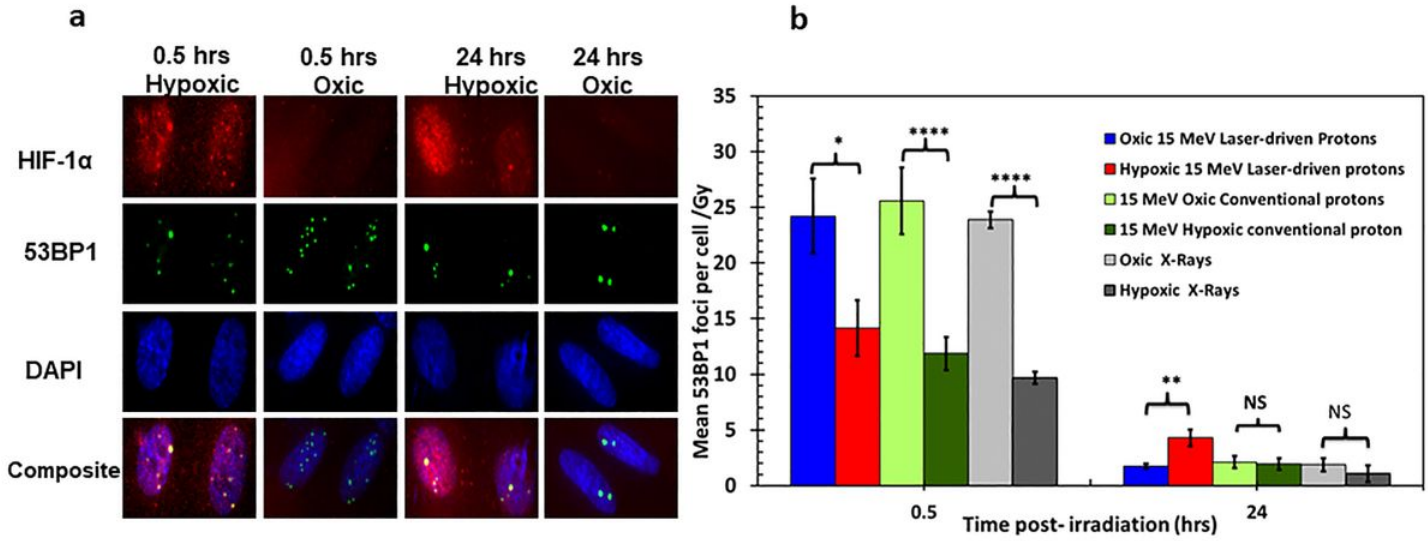

Figure 5

(a) Laser accelerated 15 MeV protons induced DNA DSB damage and repair detection using 53BP1 foci formation assay in AG01522 cells irradiated under hypoxic and oxic conditions. Cells were incubated under hypoxia for 4 hrs, irradiated, then later fixed and stained for 53BP1 foci (green) and HIF-1α (in red). (B) Quantification of laser -accelerated protons induced 53BP1 foci under oxic and hypoxic conditions for comparison cells in similar conditions were also irradiated with 1 Gy of 225 kVp X-rays. All the values on the graphs are shown after substracting the background control values. For each data point at least 100 cells in duplicate slides were analyzed and data is shown as an average of two independent replicates. Error bars represent the standard error of the mean. Statistical significance was analysed using Student's un-paired T test and * represents P values ≤0.05, *** represents P values≤ 0.0001; NS- non-significant.

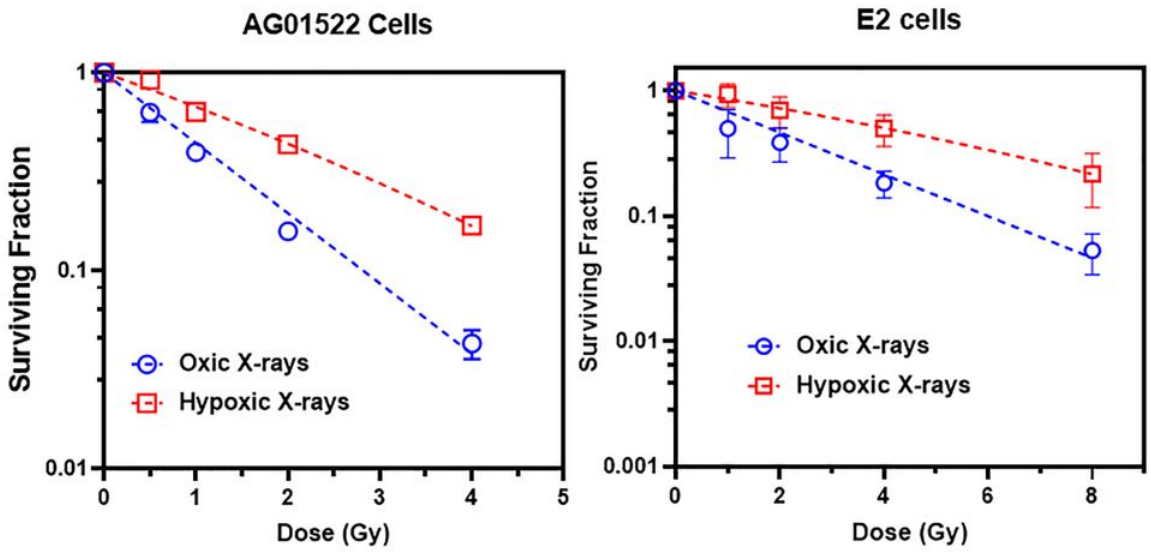

Figure 6

(a) X-rays Dose response curve of human normal skin fibroblasts (AG01522B cells) and (b) patient derived glioblastoma stem cells (E2 cells) obtained using clonogenic assay. For OER calculation various dose values resulting in surviving fraction of 10, 50 and 90 (D10,D50 and D90) were obtained as transformants on the surviving curves under oxic and hypoxic conditions. The values obtained for various doses were used to calculate OER for X –rays in both AG01522 and E2 cells as shown in the table-1.